Characterization of a Segmented n-Type Broad Energy Germanium Detector

Martin Schuster

Max-Planck Institute for Physics

March 13, 2017

Physics Motivation

Experimental Setup

Detector Characteristics

Summary & Outlook

Physics Motivation

Experimental Setup

Detector Characteristics

Summary & Outlook

Physics Motivation: $0\nu\beta\beta$ Decay

Could provide information on:

- Nature of the neutrino: Dirac or Majorana?
- Inverted or Normal Hierarchy
- Possibly hints on absolute mass scale from $T_{1/2}$

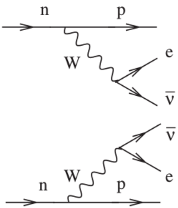

(a) $2\nu\beta\beta$

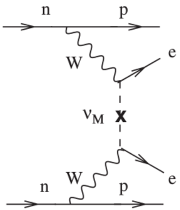

(b) $0\nu\beta\beta$

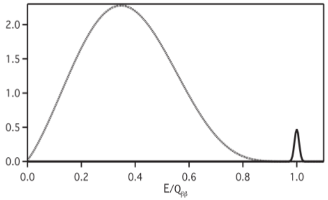

(c) Combined spectrum

Why Germanium?

- ^{76}Ge is a candidate for $0\nu\beta\beta$ and Ge is a semiconductor
- Can act as source and detector simultaneously
  $\rightarrow$ high detection efficiency
- Naturally good energy resolution
- Currently employed in experiments like GERDA and MAJORANA
- LEGEND collaboration is forming: Ton-scale germanium experiment

Physics Motivation

Experimental Setup

Detector Characteristics

Summary & Outlook

The Segmented Broad Energy Germanium Detector

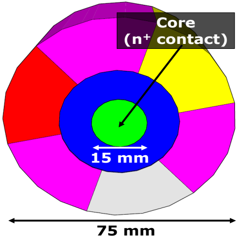

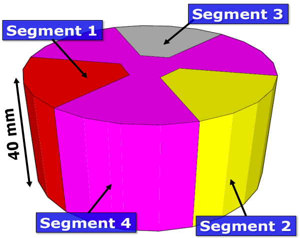

Properties

- Special electric field due to point contact: Favorable for Pulse-Shape Analysis
- Segmentation provides
  - Information on ϕ location of energy depositions
  - Complimentary background rejection

Weighting Potential

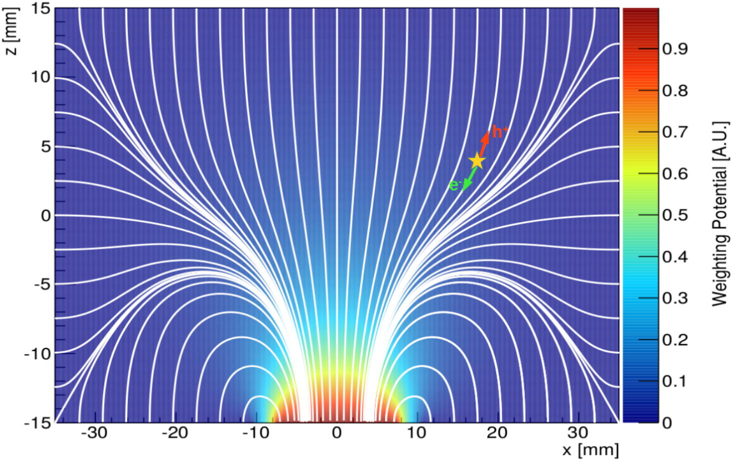

Example Pulse

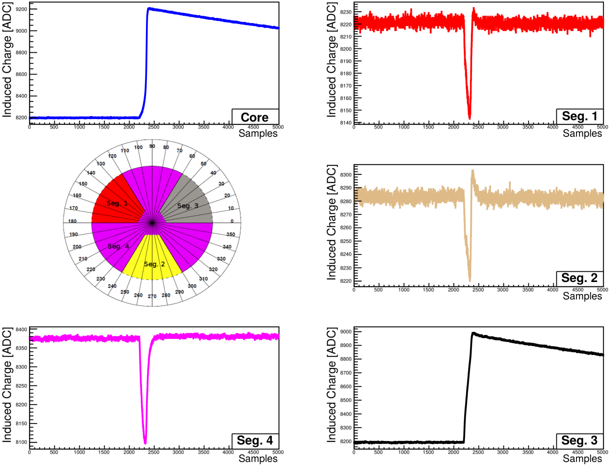

Physics Motivation

Experimental Setup

Detector Characteristics

Summary & Outlook

Crystal Axes Determination

- Slow and fast crystal axes influence the drift-path and speed of the charge carriers
- The dependence of t_{5-95} on ϕ is expected to be sinusoidal:

$$t_{5-95} = C + a \cdot \sin\left[\frac{2\pi}{90}\left(\phi + \phi_{offset}\right)\right] \quad .$$

The parameters C, a and ϕ_{offset} were fitted to the data

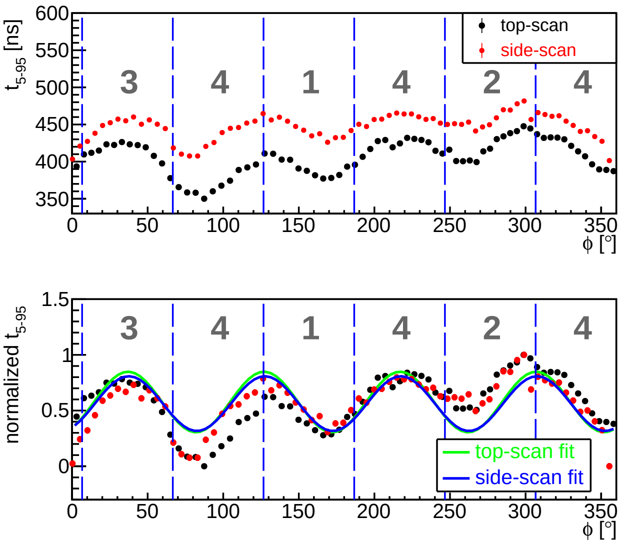

top-scan
side-scan
3 4 1 4 2 4
$t_{5\text{-}95}$ [ns]
600 550 500 450 400 350
0 50 100 150 200 250 300 350
ϕ [°]
normalized $t_{5\text{-}95}$
1.5 1 0.5 0
top-scan fit
side-scan fit

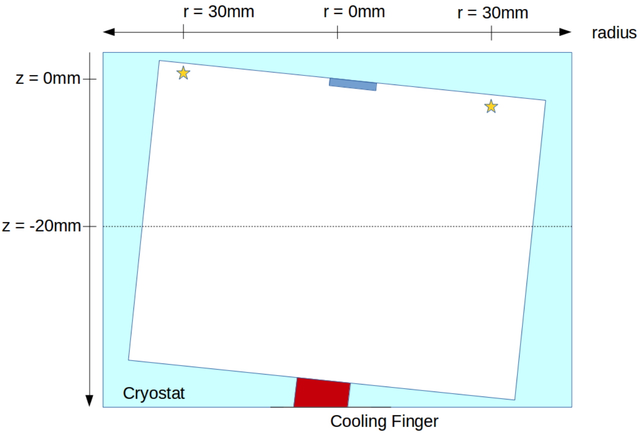
r = 30mm
r = 0mm
r = 30mm
radius
z = 0mm
z = -20mm
Cryostat
Cooling Finger

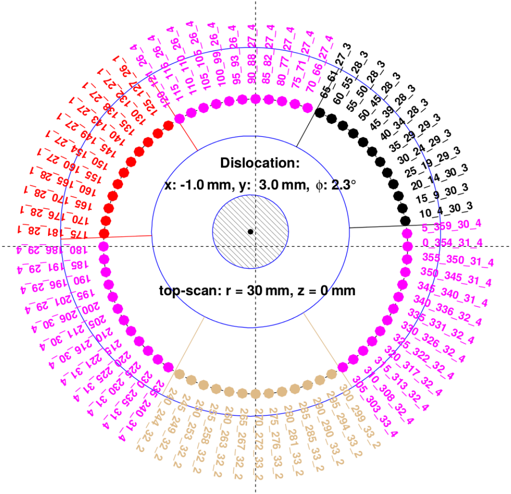
Dislocation:
x: -1.0 mm, y: 3.0 mm, ϕ: 2.3°
top-scan: r = 30 mm, z = 0 mm

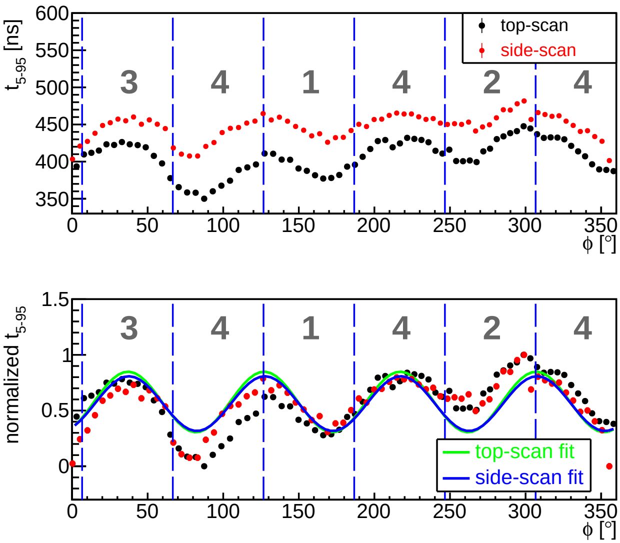

t5-95 [ns]
600
550
500
450
400
350
0
50
100
150
200
250
300
350
ϕ [°]
top-scan
side-scan
3
4
1
4
2
4
normalized t5-95
1.5
1
0.5
0
top-scan fit
side-scan fit

Localizing ϕ *Position* using Mirror Pulses

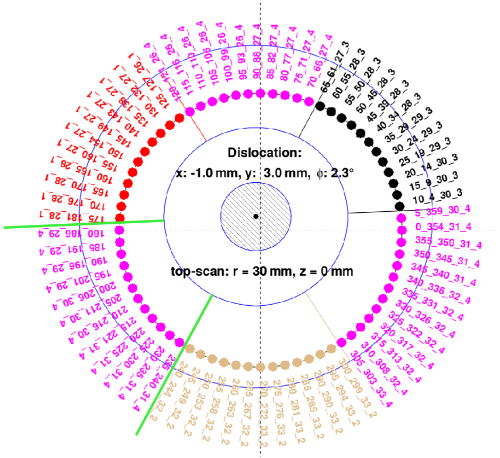

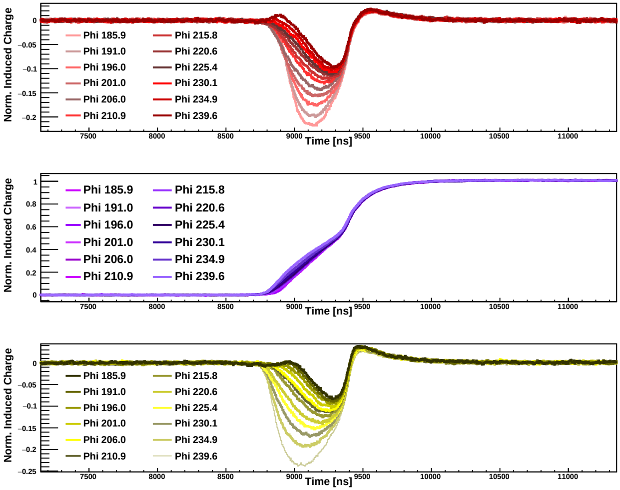
Norm. Induced Charge
Time [ns]
Phi 185.9
Phi 191.0
Phi 196.0
Phi 201.0
Phi 206.0
Phi 210.9
Phi 215.8
Phi 220.6
Phi 225.4
Phi 230.1
Phi 234.9
Phi 239.6
Norm. Induced Charge
Time [ns]
Phi 185.9
Phi 191.0
Phi 196.0
Phi 201.0
Phi 206.0
Phi 210.9
Phi 215.8
Phi 220.6
Phi 225.4
Phi 230.1
Phi 234.9
Phi 239.6
Norm. Induced Charge
Time [ns]
Phi 185.9
Phi 191.0
Phi 196.0
Phi 201.0
Phi 206.0
Phi 210.9
Phi 215.8
Phi 220.6
Phi 225.4
Phi 230.1
Phi 234.9
Phi 239.6

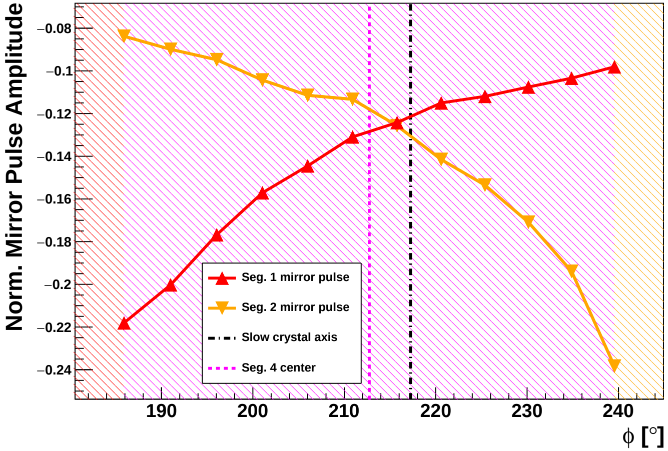
Norm. Mirror Pulse Amplitude
−0.08
−0.1
−0.12
−0.14
−0.16
−0.18
−0.2
−0.22
−0.24
190
200
210
220
230
240
ϕ [°]
Seg. 1 mirror pulse
Seg. 2 mirror pulse
Slow crystal axis
Seg. 4 center

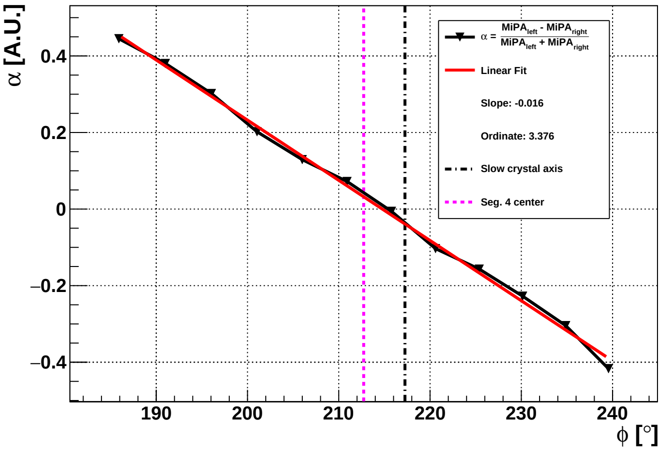
α [A.U.]
0.4
0.2
0
–0.2
–0.4
190
200
210
220
230
240
ϕ [°]
α = (MiPA_left - MiPA_right) / (MiPA_left + MiPA_right)
Linear Fit
Slope: -0.016
Ordinate: 3.376
Slow crystal axis
Seg. 4 center

Passivation Layer Studies

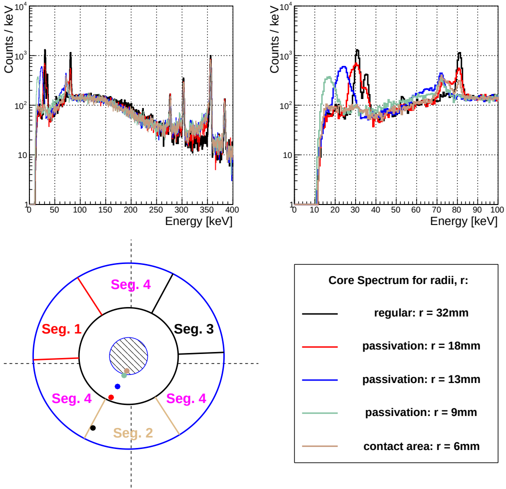

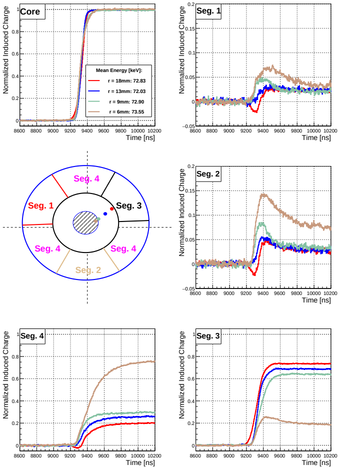

- Both segment 3 and 4 are collecting
- Truncated mirror pulses: Indication for charge trapping
- Increasing effect for smaller radii

Near Surface Effects: Distorted Field Lines

- Drift paths are bent towards the surface, where the electric field is very weak
- At surface, the charge-drift slows down significantly
- This gives rise to the obeserved phenomena via two mechanics:
  - Incomplete charge collection: Charges cease to contribute to the pulse
  - Strongly delayed pulses: Pulses don't reach their amplitude during DAQ-window

Physics Motivation

Experimental Setup

Detector Characteristics

Summary & Outlook

Summary and Results

- Prototype detector, combining the point contact layout, which is favorable for PSA with a moderate segmentation.
- Localization of the crystal axes, despite tilted installation: Good agreement between top-scans and side-scans
- Reconstructing the ϕ-position using mirror pulses of non-collecting segments: Proven to be feasible
- Indication of distorted drift paths for low energy events beneath the passivated area
  The effects show a significant r dependence, yet they are independent on ϕ

Outlook

- The detector has been moved to new, electrically cooled cryostat
- Measurements of temperature dependence of passivation layer effects and drift times in general
- Expanding and refining the event position reconstruction, including Monte-Carlo based pulse-shape libraries
- Further studies on the effect of the crystal axes

Thank you for your attention!

BACKUP

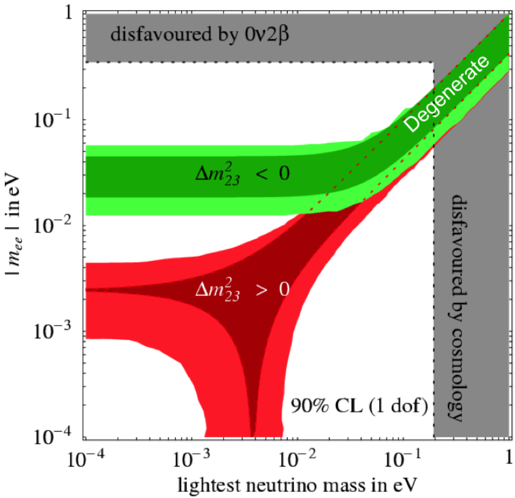

1

[1] I. Gil-Botella, Neutrino Physics (2015)

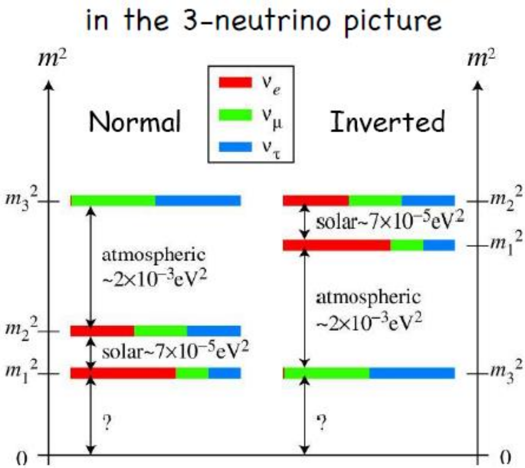
in the 3-neutrino picture
m²
Normal
Inverted
νe
νμ
ντ
m₃²
m₂²
m₁²
atmospheric
~2×10⁻³eV²
solar~7×10⁻⁵eV²
?
0

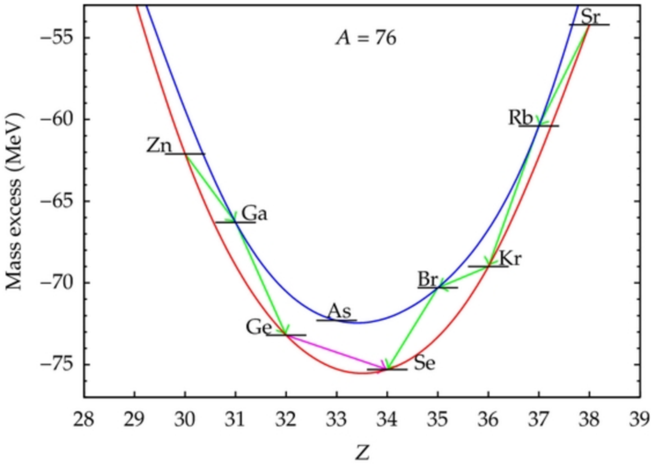

2

[2] A. Giullani and A. Poves, Advances in High Energy Physics(2012)

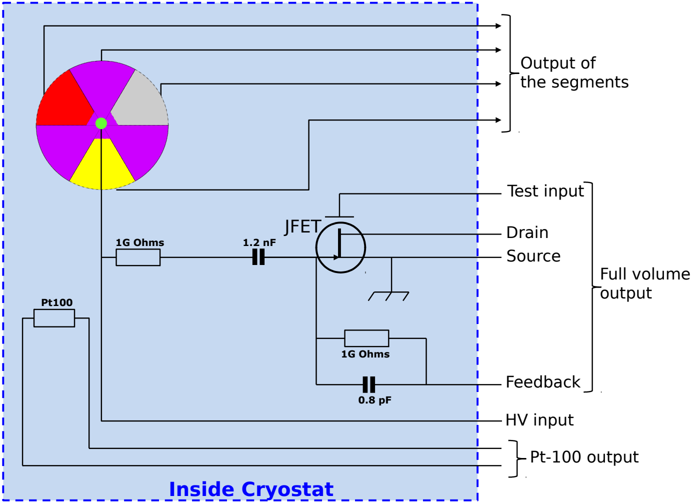
Output of
the segments
Test input
JFET
Drain
Source
1G Ohms
1.2 nF
Full volume
output
Pt100
1G Ohms
Feedback
0.8 pF
HV input
Pt-100 output
Inside Cryostat

Multi-Site- vs. Single-Site-Event Discrimination

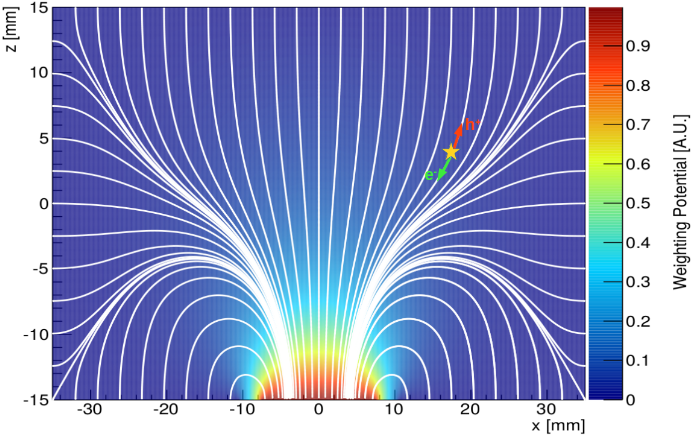

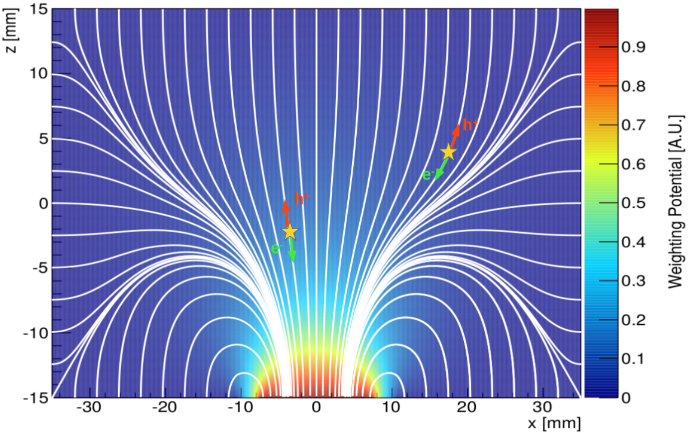

z [mm]
15
10
5
0
-5
-10
-15
-30
-20
-10
0
10
20
30
x [mm]
h+
e-
h+
e-
0.9
0.8
0.7
0.6
0.5
0.4
0.3
0.2
0.1
0
Weighting Potential [A.U.]

A/E Method

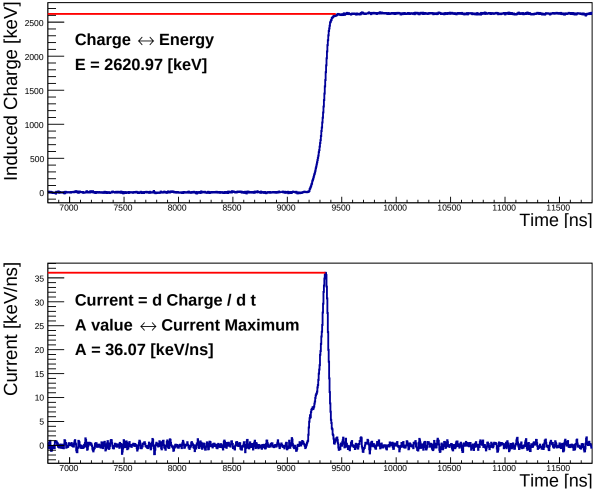
Induced Charge [keV]
2500
2000
1500
1000
500
0
Charge ↔ Energy
E = 2620.97 [keV]
7000 7500 8000 8500 9000 9500 10000 10500 11000 11500
Time [ns]
Current [keV/ns]
35
30
25
20
15
10
5
0
Current = d Charge / d t
A value ↔ Current Maximum
A = 36.07 [keV/ns]
7000 7500 8000 8500 9000 9500 10000 10500 11000 11500
Time [ns]

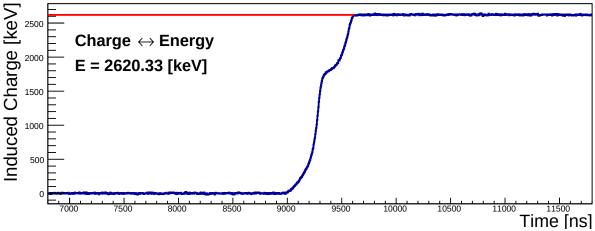
Induced Charge [keV]
Charge ↔ Energy
E = 2620.33 [keV]
2500
2000
1500
1000
500
0
7000 7500 8000 8500 9000 9500 10000 10500 11000 11500
Time [ns]

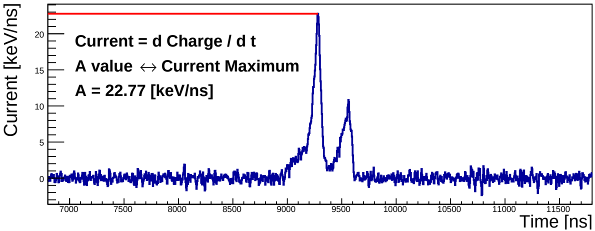
Current [keV/ns]
Current = d Charge / d t
A value ↔ Current Maximum
A = 22.77 [keV/ns]
20
15
10
5
0
7000 7500 8000 8500 9000 9500 10000 10500 11000 11500
Time [ns]

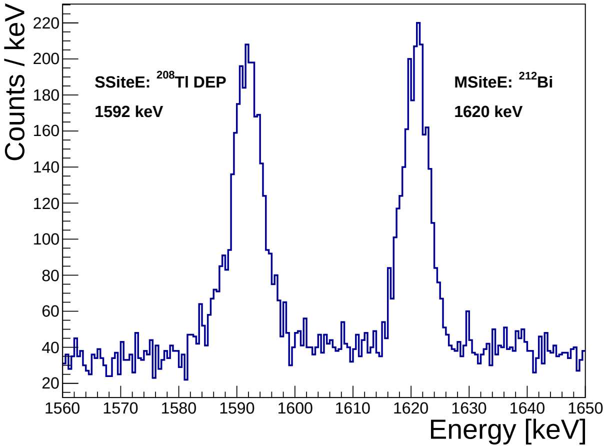

Counts / keV
220
200
180
160
140
120
100
80
60
40
20
SSiteE: 208Tl DEP
1592 keV
MSiteE: 212Bi
1620 keV
1560
1570
1580
1590
1600
1610
1620
1630
1640
1650
Energy [keV]

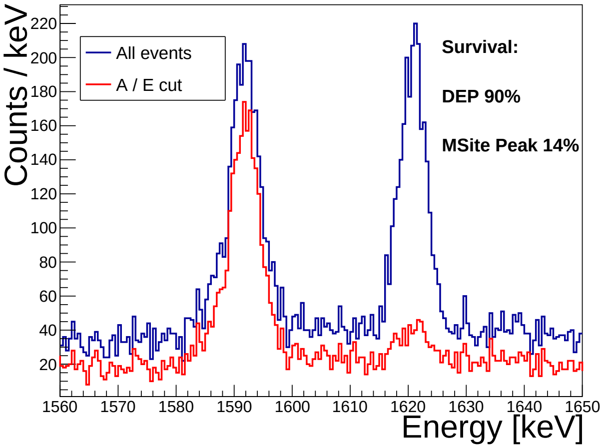
Counts / keV
220
200
180
160
140
120
100
80
60
40
20
All events
A / E cut
Survival:
DEP 90%
MSite Peak 14%
1560
1570
1580
1590
1600
1610
1620
1630
1640
1650
Energy [keV]

Segmentation Cut

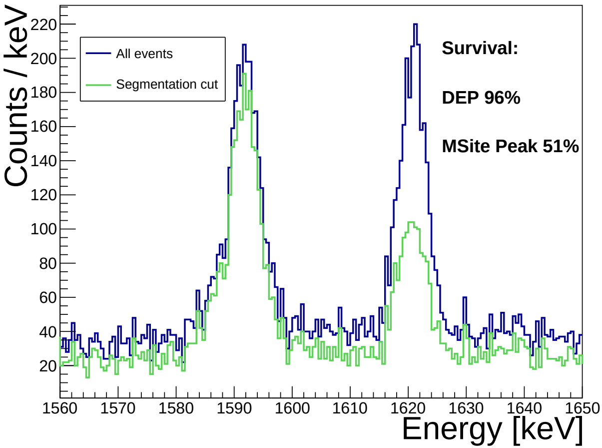

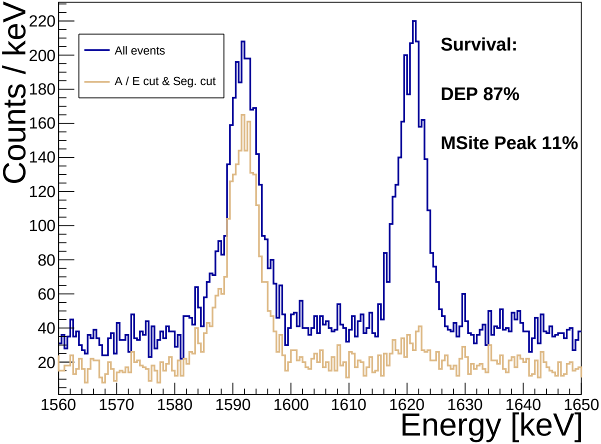
Counts / keV
220
200
180
160
140
120
100
80
60
40
20
All events
A / E cut & Seg. cut
Survival:
DEP 87%
MSite Peak 11%
1560
1570
1580
1590
1600
1610
1620
1630
1640
1650
Energy [keV]

Example Core Pulse as provided by the ADC

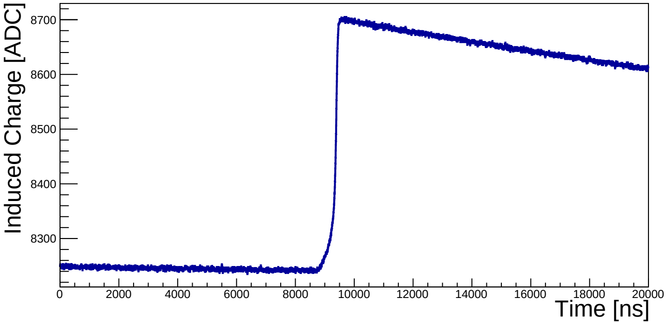

Fixed Window Method for Pulse Amplitude Determination

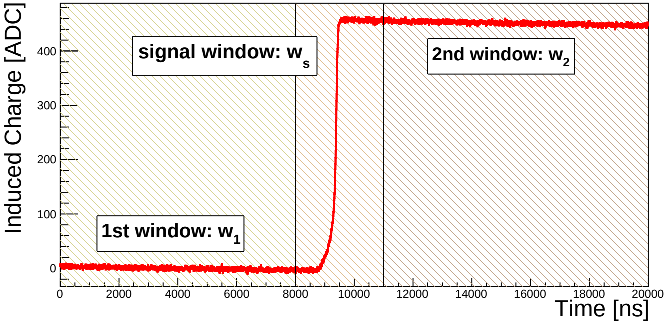

The matrix c^*_{ij} links the true energy E_i^{true} and the measured pulse amplitudes M_i:

$$\begin{pmatrix} E_0^{true} & \dots & E_4^{true} \end{pmatrix} \cdot \begin{pmatrix} c^*_{00} & \dots & c^*_{04} \\ \vdots & \ddots & \vdots \\ c^*_{40} & \dots & c^*_{44} \end{pmatrix} = \begin{pmatrix} M_0 & \dots & M_4 \end{pmatrix} \quad .$$

E_i^{true} can be determined using the inverse matrix ${c^*_{ij}}^{-1}$:

$$\begin{pmatrix} E_0^{true} & \dots & E_4^{true} \end{pmatrix} = \begin{pmatrix} M_0 & \dots & M_4 \end{pmatrix} \cdot \begin{pmatrix} c^*_{00} & \dots & c^*_{04} \\ \vdots & \ddots & \vdots \\ c^*_{40} & \dots & c^*_{44} \end{pmatrix}^{-1} \quad .$$

$$M_0 = E_0^{true} \cdot c_{00}^* + E_1^{true} \cdot c_{10}^* + \ldots + E_4^{true} \cdot c_{40}^* \quad . \qquad (1)$$

By introducing the assumption that the cross-talk from the segments to the core is the same for all the segments, $c_{10}^* = c_{i0}^*$, $i \in \{2, 3, 4\}$ and using the identity $\sum_{i=1}^{4} E_i^{true} = E_0^{true}$, M_0 becomes:

$$M_0 = E_0^{true} \cdot (c_{00}^* + c_{10}^*) \qquad (2)$$

$$= E_0^{true} \cdot c^{core} \quad . \qquad (3)$$

The value of the thus defined c^{core} can be determined by the standard procedure of fitting the core spectrum with the known photon lines using all events.

The cross-talk from the core to the segments can mathematically be unified with the segment to segment cross-talk. For demonstration, consider the measured pulse amplitude for segment 1, M_1. Again making use of the identity $\sum_{i=1}^{4} E_i^{true} = E_0^{true}$:

$$M_1 = \sum_{i=0}^{4} E_i^{true} \cdot c_{i1}^{*} \tag{4}$$

$$= E_0^{true} \cdot c_{01}^{*} + \sum_{i=1}^{4} E_i^{true} \cdot c_{i1}^{*} \tag{5}$$

$$= \sum_{i=1}^{4} E_i^{true} \cdot c_{01}^{*} + \sum_{i=1}^{4} E_i^{true} \cdot c_{i1}^{*} \tag{6}$$

$$= \sum_{i=1}^{4} E_i^{true} (c_{01}^{*} + c_{i1}^{*}) = \sum_{i=1}^{4} E_i^{true} \cdot c_{i1} \quad . \tag{7}$$

Reduced matrix c_{ij}, $i, j \in \{1, 2, 3, 4\}$ and the equations:

$$M_0 = E_0^{true} \cdot c^{core} \quad (8)$$

$$\begin{pmatrix} M_1 & \dots & M_4 \end{pmatrix} = \begin{pmatrix} E_1^{true} & \dots & E_4^{true} \end{pmatrix} \cdot \begin{pmatrix} c_{11} & \dots & c_{14} \\ \vdots & \ddots & \vdots \\ c_{41} & \dots & c_{44} \end{pmatrix} . \quad (9)$$

The matrix elements c_{ij} can be determined by investigating single-segment events.

For single-segment i events, $E_i^{true} = E_0^{true}$, $E_{j \neq i}^{true} = 0$. Using segment 1 as an example, the measured pulse amplitude for single-segment 1 events, M_1, can then be written as:

$$M_1 = E_1^{true} \cdot c_{11} + E_2^{true} \cdot c_{21} + E_3^{true} \cdot c_{31} + E_4^{true} \cdot c_{41} \tag{10}$$
$$= E_1^{true} \cdot c_{11} + 0 \cdot c_{21} \ldots \tag{11}$$

In general, for single-segment i events, $M_i = E_i \cdot c_{ii}$, $i \in \{1, 2, 3, 4\}$. Then the matrix elements c_{ii} can be determined:

$$c_{ii} = \frac{M_i}{E_i^{true}} = \frac{M_i}{E_0^{true}} = \frac{M_i \cdot c^{core}}{M_0} \tag{12}$$
$$= R^{ssi} \cdot c^{core} \quad . \tag{13}$$

After the cross-talk correction and energy calibration procedure, Tab 1 gives an overview of the energy resolutions for selected γ-lines and all the segments.

		FWHM [keV]				
Source	**γ-line [keV]**	**Core**	**Seg. 1**	**Seg. 2**	**Seg. 3**	**Seg. 4**
^{133}Ba	81	3.29	5.15	4.05	4.07	7.26
	356	2.64	4.58	3.47	3.52	6.04
^{60}Co	1173	4.57	4.88	4.16	4.34	8.05
	1332	4.93	5.00	4.39	4.14	7.84
^{228}Th	2614	7.65				

Table: Energy resolutions as absolute FWHM in keV. The resolutions for especially characteristic γ-lines for the respective sources are given.

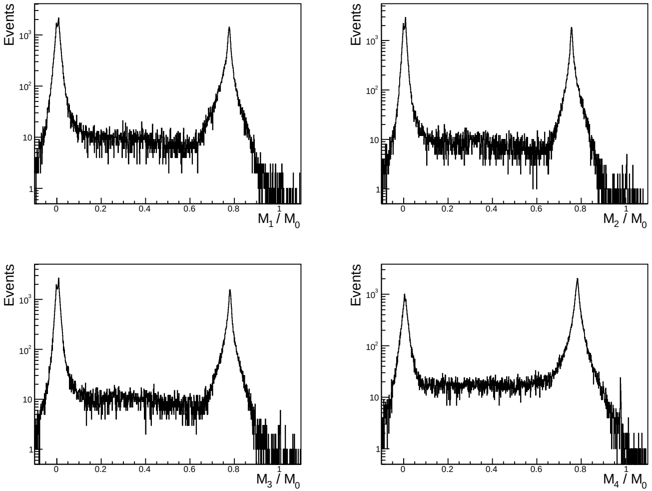
Events
M1 / M0
Events
M2 / M0
Events
M3 / M0
Events
M4 / M0
0
0.2
0.4
0.6
0.8
1
1
10
10^2
10^3

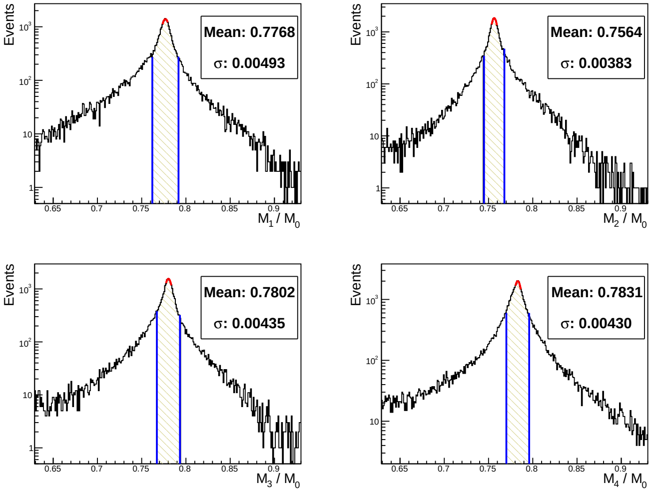
Events
Mean: 0.7768
σ: 0.00493
M_1 / M_0
Events
Mean: 0.7564
σ: 0.00383
M_2 / M_0
Events
Mean: 0.7802
σ: 0.00435
M_3 / M_0
Events
Mean: 0.7831
σ: 0.00430
M_4 / M_0

The remaining matrix elements can also be determined studying single-segment events. For single-segment i events, the measured pulse amplitudes in the other segments $j, j \neq i$, can be written as:

$$M_j = E_i^{true} \cdot c_{ij} \quad , \tag{14}$$

and the ratio between M_j and M_i, $m_{ji} = M_j / M_i$, leads to:

$$m_{ji} = \frac{E_i^{true} \cdot c_{ij}}{E_i^{true} \cdot c_{ii}} = \frac{c_{ij}}{c_{ii}} \tag{15}$$

$$\Rightarrow c_{ij} = m_{ji} \cdot c_{ii} \quad . \tag{16}$$

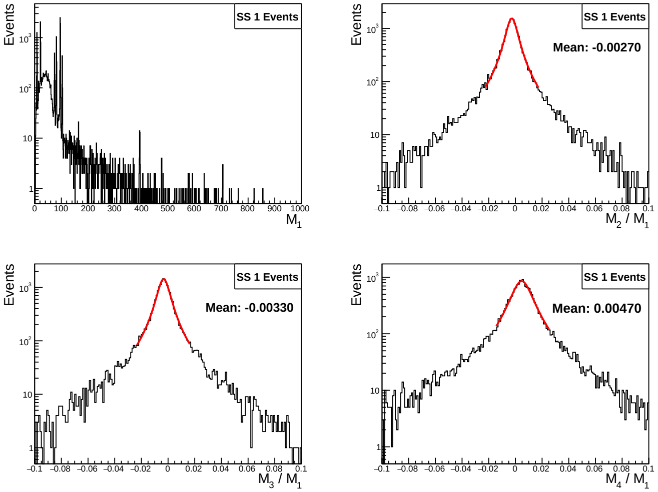
Events
SS 1 Events
M_1
Mean: -0.00270
M_2 / M_1
Mean: -0.00330
M_3 / M_1
Mean: 0.00470
M_4 / M_1

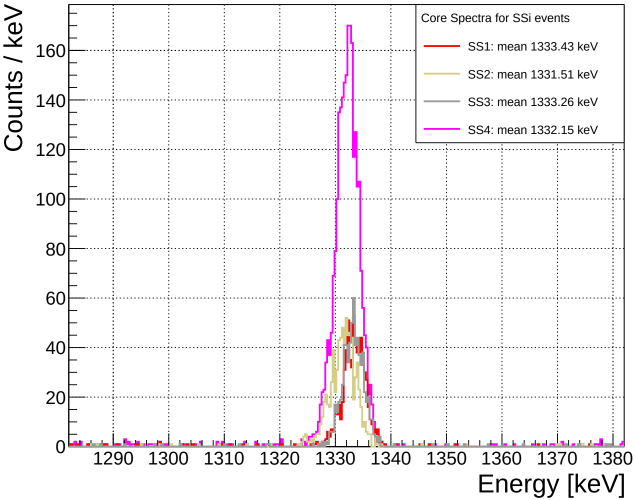
Core Spectra for SSi events
SS1: mean 1333.43 keV
SS2: mean 1331.51 keV
SS3: mean 1333.26 keV
SS4: mean 1332.15 keV
Counts / keV
Energy [keV]
0
20
40
60
80
100
120
140
160
1290
1300
1310
1320
1330
1340
1350
1360
1370
1380

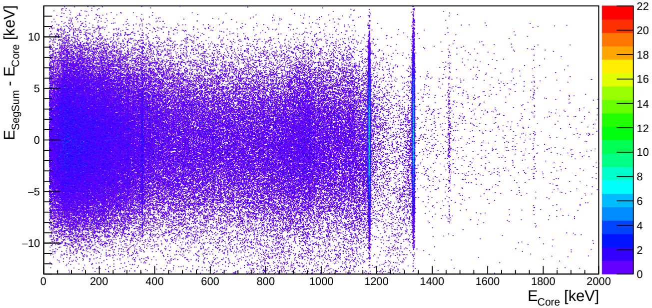

E_SegSum - E_Core [keV]
10
5
0
−5
−10
0
200
400
600
800
1000
1200
1400
1600
1800
2000
E_Core [keV]
22
20
18
16
14
12
10
8
6
4
2
0

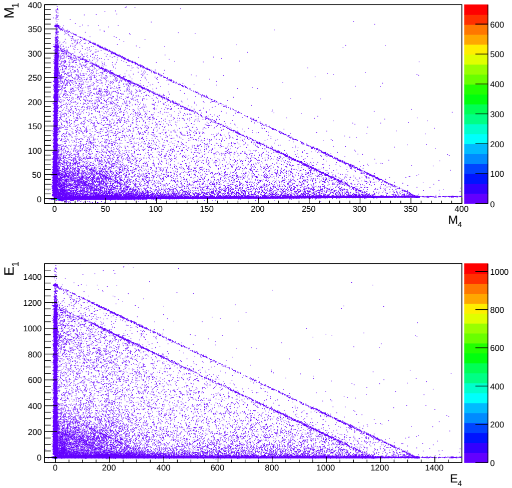

M1
M4
E1
E4

Segment	Boundary(i, j)	Top-scan	Side-scan
1	$\phi_{4,1}$	124.7 ± 0.6	120.0 ± 0.8
	$\phi_{1,4}$	181.1 ± 0.6	181.1 ± 0.8
2	$\phi_{4,2}$	244.0 ± 0.6	242.5 ± 0.7
	$\phi_{2,4}$	302.5 ± 0.6	302.1 ± 0.8
3	$\phi_{4,3}$	7.1 ± 0.5	3.8 ± 0.7
	$\phi_{3,4}$	64.8 ± 0.6	63.5 ± 0.7
4	$\phi_{3,4}$	66.6 ± 0.6	62.8 ± 0.7
	$\phi_{4,1}$	123.0 ± 0.6	120.2 ± 0.8
	$\phi_{1,4}$	182.5 ± 0.5	180.8 ± 0.7
	$\phi_{4,2}$	242.4 ± 0.6	242.3 ± 0.6
	$\phi_{2,4}$	303.2 ± 0.8	302.0 ± 0.7
	$\phi_{4,3}$	6.2 ± 0.5	3.4 ± 0.6

Scan	ϕ_{offset}	$\phi_{\langle 110 \rangle}$
Top	-14.52 $\pm$ 0.24	37.02 $\pm$ 0.24
Side	-15.05 $\pm$ 0.30	37.55 $\pm$ 0.30

Table: The values of ϕ_{offset} and $\phi_{\langle 110 \rangle}$, see Eq. 11, as determined by fits to the data.

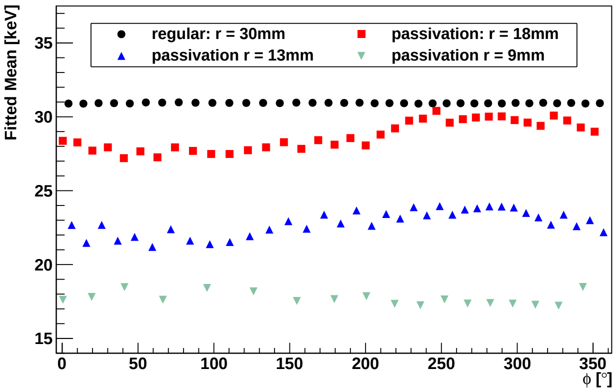

regular: r = 30mm
passivation: r = 18mm
passivation r = 13mm
passivation r = 9mm
Fitted Mean [keV]
35
30
25
20
15
0
50
100
150
200
250
300
350
ϕ [°]

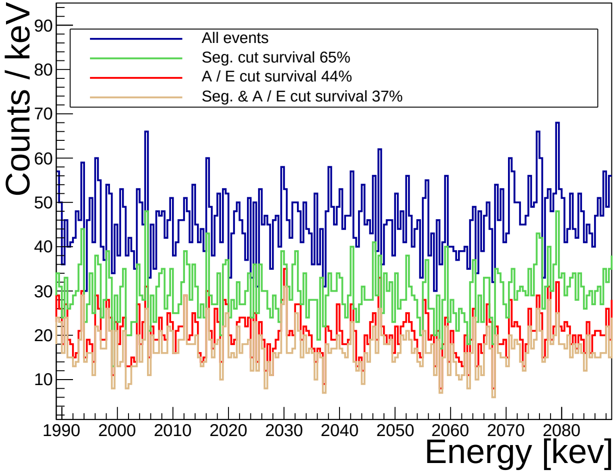
All events
Seg. cut survival 65%
A / E cut survival 44%
Seg. & A / E cut survival 37%
Counts / keV
10
20
30
40
50
60
70
80
90
1990
2000
2010
2020
2030
2040
2050
2060
2070
2080
Energy [kev]